JOURNAL OF GEOPHYSICAL RESEARCH, VOL. 99, NO. B2, PAGES 3015–3029, FEBRUARY 10, 1994

Three-dimensional gravity study of the Mid-Atlantic Ridge: Evolution of the segmentation between 28° and 29°N during the last 10 m.y.

C. Rommevaux, C. Deplus, and P. Patriat
Institut de Physique du Globe, Paris

J.-C. Sempéré
School of Oceanography, University of Washington, Seattle

During the high-resolution survey SARA (Segmentation Ancienne de la Ride Atlantique), Sea Beam bathymetry, magnetic, gravity, and seismic reflection data were collected on the flanks of the Mid-Atlantic Ridge, between 28° and 29°N. This survey was designed to provide off-axis information (up to approximately 10 m.y.) and to complement a detailed on-axis survey carried out in 1988 and 1989 (Sempéré et al., 1990) between the Atlantis and Kane fracture zones. A previous gravity study had revealed the existence of "bulls-eye" shaped gravity lows centered on the axial segments and gravity highs centered on the non-transform discontinuities (Lin et al., 1990). We carried out a three-dimensional calculation of the mantle Bouguer anomaly in order to investigate if the axial pattern of circular anomaly lows can be followed on the flanks of the spreading center. The off-axis gravity anomalies are characterized by anomaly lows over the centers of the segments and anomaly highs over the discontinuities. After correcting for the gravity effect of lithospheric cooling away from the ridge, the segmentation configuration determined from gravity data appears to be very similar to that deduced from bathymetry. Off-axis bathymetry is characterized by southward pointing, V-shaped basins which indicate that the traces of the nontransform discontinuities do not follow plate motion flow lines and that each ridge segment advances and retreats continuously. However, the gravity trace of the discontinuities is always slightly offset with respect to the bathymetric lows: northward on the western flank and southward on the eastern flank. The sense of offset between the gravity and bathymetric traces appears to be related to the right-stepping nature of the axial discontinuities.

INTRODUCTION

Most geophysical studies over mid-oceanic ridges, particularly over the Mid-Atlantic Ridge (MAR) north and south of the equator, have been carried out over lithosphere less than 2 m.y. old. Multibeam bathymetry, gravity, and magnetic data have been collected to map the axes of the mid-ocean ridge and to study the processes governing the creation of oceanic crust. These studies have shown that the spreading axis, between two large transform faults, consists of a narrow volcanic zone, segmented by nontransform discontinuities with an offset typically less than 20 km [*Macdonald et al.*, 1991]. Three-dimensional gravity studies have been carried out over the axis of the MAR [*Kuo and Forsyth*, 1988; *Lin et al.*, 1990; *Morris and Detrick*, 1991]. In these studies, the mantle Bouguer anomaly was computed by removing from the free-air anomaly the gravity effect of the topography and the Moho interface, assuming a constant crustal thickness and density. In these studies, the effect of lithospheric cooling was subtracted using the method of *Phipps Morgan and Forsyth* [1988] and *Kuo and Forsyth* [1988]. The residual anomalies showed closed-contour gravity lows centered over tectonically defined spreading segments. These anomalies have been interpreted in terms of along-axis variations in crustal thickness and/or density anomalies in the crust or upper mantle that are associated with focused upwelling of mantle beneath the middle of ridge segments [*Kuo and Forsyth*, 1988]. In order to study the temporal evolution of this axial segmentation, the SARA (Segmentation Ancienne de la Ride Atlantique) cruise extended the survey of *Sempéré et al.* [1990] (RC2912) on the flanks between 28° and 29°N out to 10 Ma (Figure 1). Sea Beam bathymetry, magnetic, gravity, and seismic reflection data were collected on board R/V *Jean Charcot* (May 1990) along a series of profiles oriented along the present flow lines (110°). In this paper, we present the three-dimensional analysis of gravity anomalies off axis. This method allows us to investigate whether the mantle Bouguer anomalies can be followed off axis and to study the temporal evolution of the ridge segmentation.

Paper number 93JB02361.
0148-0227/94/93JB-02361$05.00

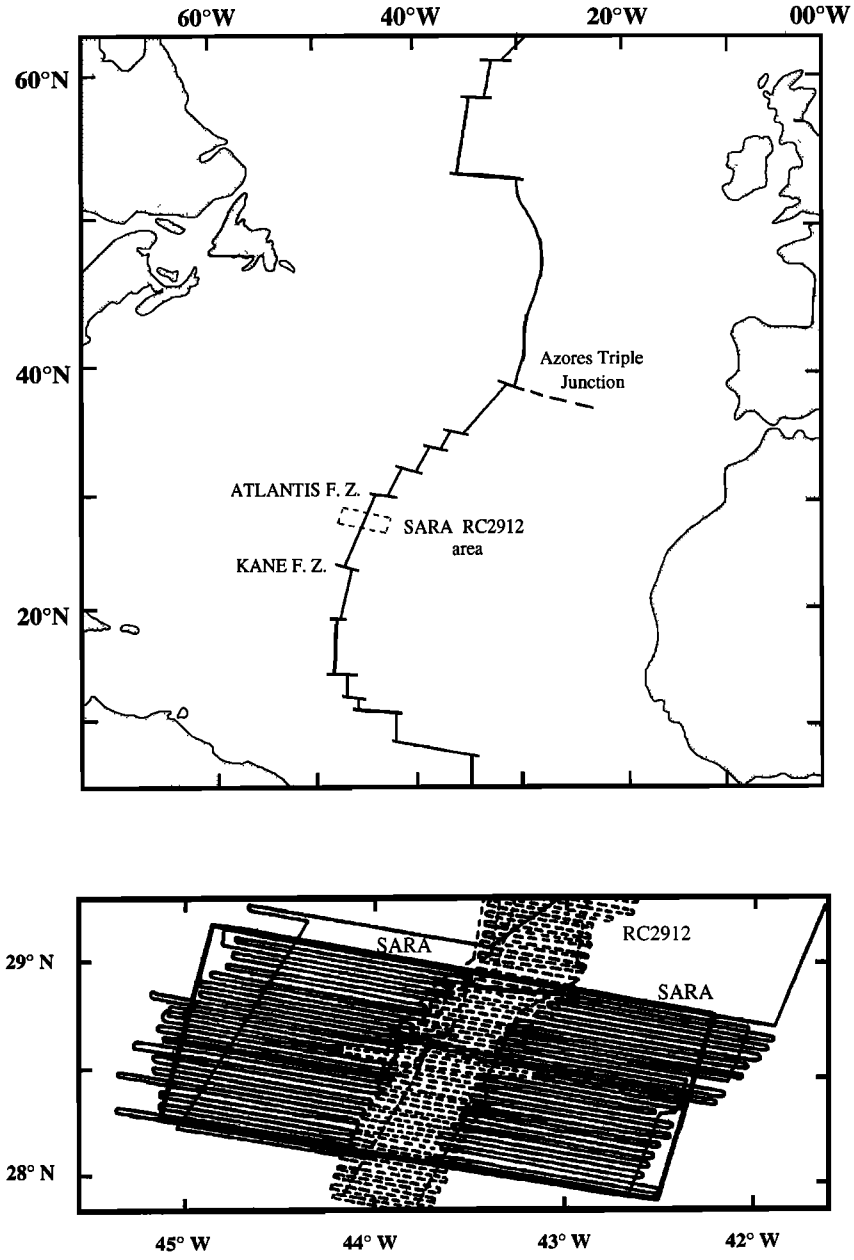

Fig. 1. General setting of study area, and map of track lines from the RC2912 (dashed lines) and SARA (solid lines) Cruises where bathymetry Seabeam, gravity and magnetic data were collected. Heavy solid-line box indicates the grid area used in the three dimensional gravity study.

BATHYMETRY

Plate 1a shows the bathymetric map of the survey area (see Figure 1 for limits), contoured at 200 m intervals. The along-axis spreading center morphology consists of an axial valley with a mean depth of 3500 m and a succession of topographic highs and lows. This axial topography is generally interpreted in terms of segments and discontinuities. Three segments, with lengths varying from 29 to 61 km, offset by nontransform discontinuities (NTDs) have been identified in this area [*Sempéré et al.*, 1990]. The offset between adjacent segments varies from 3 to 7 km. The topography on both flanks is formed by a series of topographic lows and highs that parallel the axis. The most striking features in the ridge flank bathymetry are a series of elongated oblique depressions (about 3000 m in depth) that form broad V shapes pointing south. Seismic reflection data reveal that these depressions, which appear flat-bottomed in bathymetric data, are in fact small basins filled with up to 400 m of sediment (Figure 2). These topographic lows which are correlated with magnetic anomaly identification gaps (Plate 1a), are interpreted as the fossil traces of the NTDs [*Patriat et al.*, 1990]. Between anomalies 5 and 4a, these basins on both flanks consist of a narrow zone of lineations oblique to the axial trend of the axis [*Sloan and Patriat*, 1992]. Isochrons 5 and 4a are offset by about 23 km. These observations suggest that between anomalies 5 and 4a, the ridge axis consisted of only two segments and

was offset by a small transform fault. From anomaly 4a to the present, previously created large basins were split into two separate, elongated basins enclosing a new segment (between 28°35'N, 44°40'W and 28°20'N, 42°40'W on Plate 1a). These bathymetric and magnetic features indicate that the axial configuration has evolved during the last 10 m.y., including the initiation of a new segment at anomaly 4a time, and lengthening and/or shortening of segments, as shown in Plate 1a. This change of axial configuration has created "zigzag" traces on the flanks of the spreading center which are not parallel to the directions of either relative or absolute plate motion.

FREE AIR ANOMALY

The gravity data used in this study were collected during the leg SARA with a KSS-30 Bodenseewerk gravimeter on board the R/V *Jean Charcot* and with a BGM-3 gravimeter during leg RC2912 on board the R/V *Robert Conrad.* Navigation was accomplished using 20 hours of Global Positioning System (GPS) per day during leg SARA and 6-7 hours/d during leg RC2912 and by transit satellite fixes during the intervals without GPS. The navigation error for both cruises is estimated at about 60 m from bathymetric cross-over errors. The gravity measurements were tied to the International Gravity Standardization Net 1971 reference system (IGSN71). The mean drift of the BGM-3 gravimeter was calculated to be 2.3 mGal/month, based on a comparison of gravity values at a reference station in Cadiz (Spain) and in Punta Delgada (Azores) before and after the cruise. The mean drift of the KSS-30 was determined to be 1.7 mGal/month by comparing gravity values at a reference station in Punta Delgada (Azores) before and after the cruise. After applying the Eötvös correction and accounting for instrument drift, gravity values were then reduced to free-air anomalies (FAA) by removing the theoretical field (IGSN71). On each profile, data were sampled every minute. Analysis of survey line cross-over points for the two cruises reveals that more than 74% of the FAA discrepancies at crossing points are less than ±2 mGal. We thus estimate that the accuracy of our data is better than ± 2 mGal (Figure 3).

Pate 1b shows the FAA map, contoured at intervals of 5 mGal. The anomaly ranges from -20 mGal over the median valley to 100 mGal on the flanks. As expected, the free-air anomaly is very well correlated with bathymetry because of the large contribution of the seafloor topography to the gravity signal. Anomaly minima are associated with the greater seafloor depths: deep off-axis basins and on-axis morphological discontinuities appear clearly on the map (purples and blues on Plate 1b). Positive anomalies are associated with topographic highs on the flanks. To investigate the subseafloor structure, we calculated the mantle Bouguer anomaly by removing the predicted gravity signal associated with the seafloor topography and Moho.

THREE-DIMENSIONAL GRAVITY STUDY

Gravity Computation

To calculate the gravity anomaly due to a crustal model, we use a direct three-dimensional calculation based on the algorithm of *Chapman* [1979]. In this method, the shape of the studied body can be described by polyhedrons of constant density, whose surfaces are composed of a number of planar facets. We calculate the gravity anomaly for each polyhedron using the fundamental integral formula:

$$g(x,y,z) = \rho G \iiint_V \frac{(z-z')dx'\,dy'\,dz'}{\left((x-x')^2+(y-y')^2+(z-z')^2\right)^{3/2}}$$

where z is along the vertical upward direction, (x, y, z) refers to a point external to the volume V of the polyhedron, (x', y', z') is a point inside the polyhedron or on its boundary, G is the gravitational constant, and ρ the density.

We simplify the calculation by converting the volume integral to a summation of surface integrals each of which corresponds to a planar facet of the polyhedron. For every observation point, the contribution of each facet is computed and then summed to obtain the gravity effect due to the entire body. This method has been used to model the gravity anomaly over a seamount near the Japan Trench [*Dubois and Deplus*, 1989]. In the present study, the effect of each density interface is computed as a series of triangular facets defined by points on a rectangular grid at the depth of the interface. In order to reduce edge effects, rectangular facets of 100 km in length were added onto the edges of the grid. To define a polyhedron, a horizontal reference plane with an arbitrary depth is added. Changing the depth of this plane leads to add a constant value in the computed anomaly. Therefore, the mean value of our computed anomaly is arbitrary and we will remove it in the following computations to emphasize amplitude variations.

To generate grids, we used an algorithm based upon the cubic B spline method of *Inoue* [1986]. In this method the degree of smoothing is determined by two parameters: roughness and tension, which control the trade-off between the approximation of data and the total smoothness. We chose a high value of roughness (10,000) and a tension of 0.75 because of the high quality of the data. The grid size was chosen in order to use the part of the study area where the data density is homogeneous (Figure 1). To best minimize the possibility of creating interpolation artefacts, the grid interval is equivalent to the spacing of the profiles (2.8 km), which leads to a 36x96 grid.

In order to compute the mantle Bouguer anomaly, the following model of the oceanic crust was used (Figure 4a):

1. The seafloor is modeled using the bathymetric data.

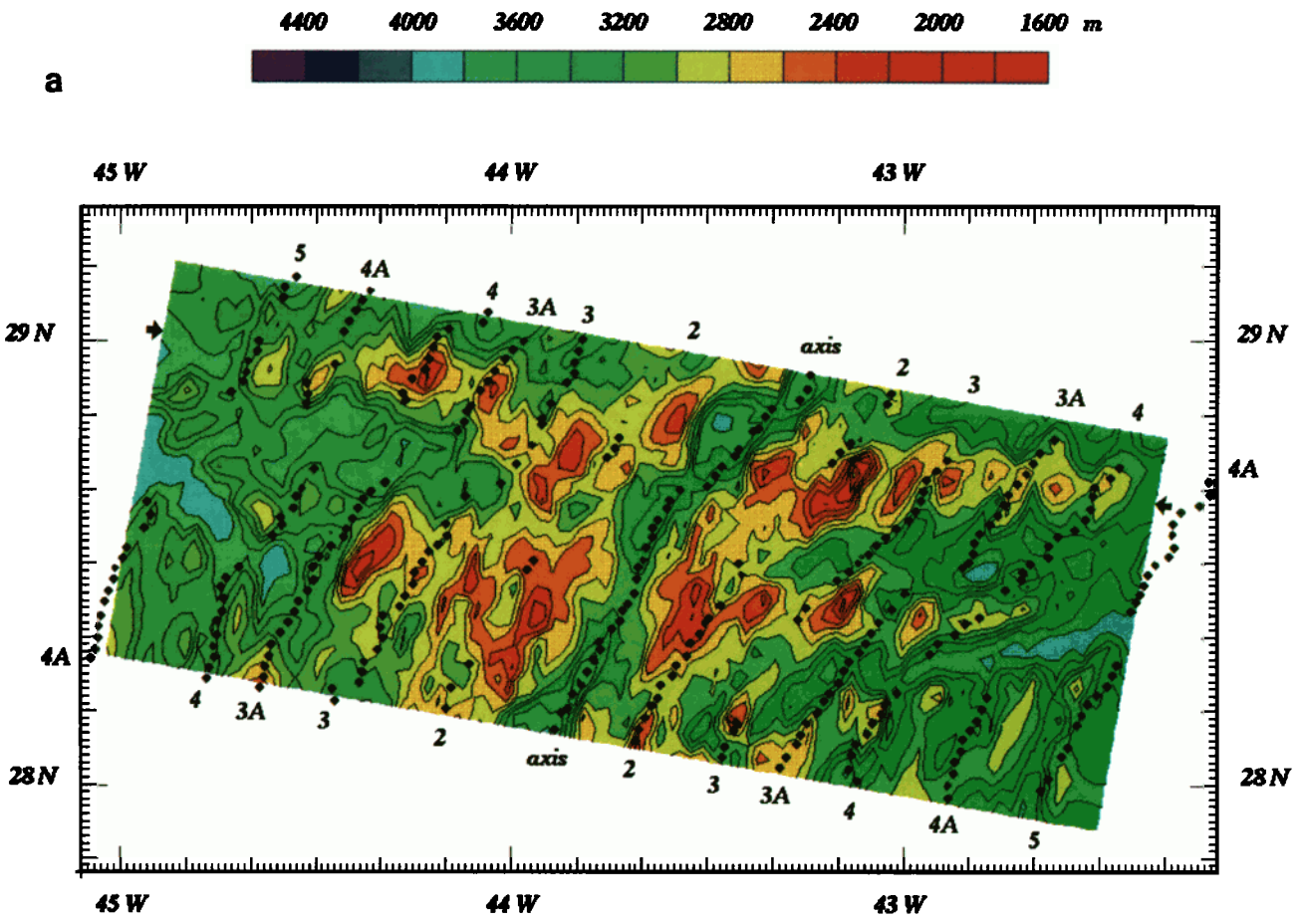
a
4400 4000 3600 3200 2800 2400 2000 1600 m
45 W
44 W
43 W
29 N
28 N
4A
5
4A
4
3A
3
2
axis
2
3
3A
4
4
3A
3
2
axis
2
3
3A
4
4A
5

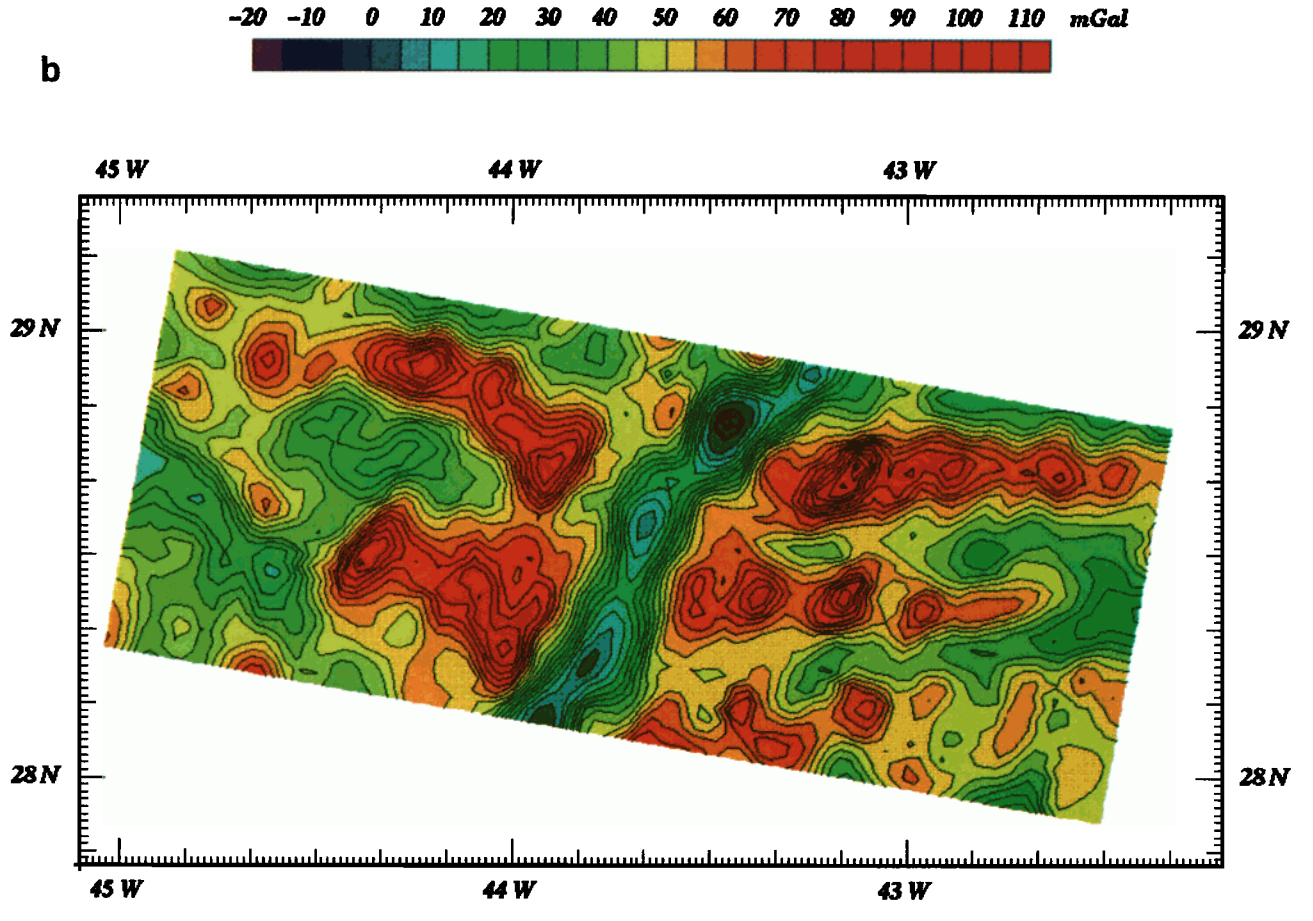
b
-20 -10 0 10 20 30 40 50 60 70 80 90 100 110 mGal
45 W
44 W
43 W
29 N
28 N

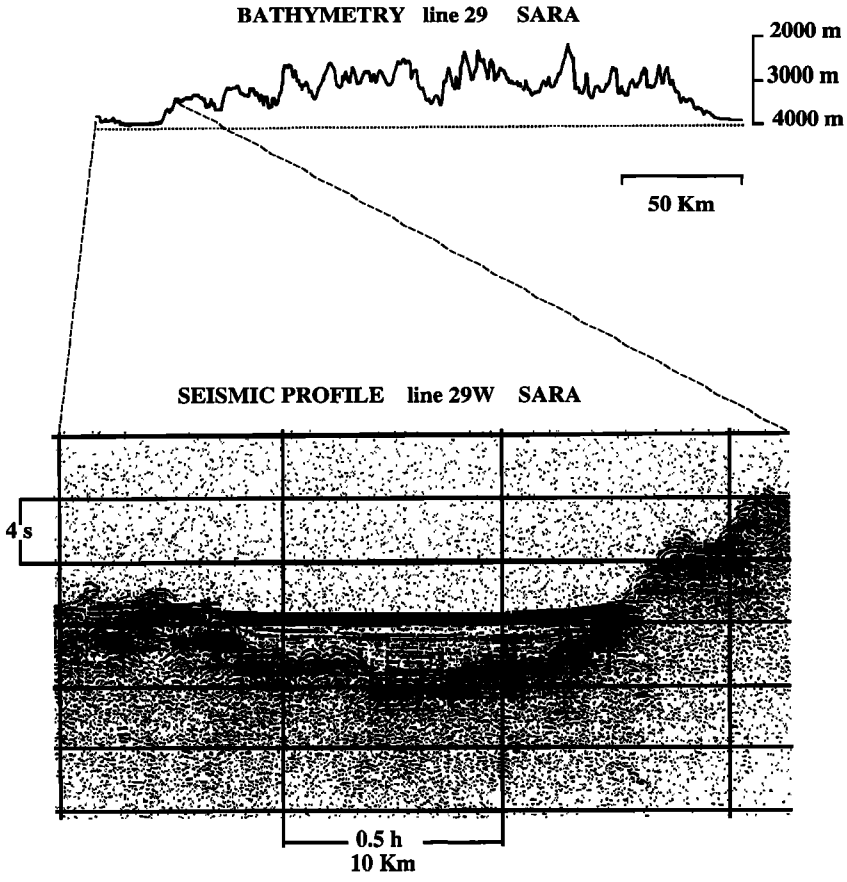

Fig. 2. Bathymetric and seismic reflection profiles located along line 29. The location of this line is shown in Plate 1a. The basin on the west flank is filled with 400 m of sediment, assuming a sediment velocity of 2 km/s.

2. The depth to the basement is defined by the sediment thickness determined by assuming a mean sediment velocity of 2 km/s.
3. A crust of constant thickness (5000 m) with the Moho following the bathymetry is assumed.

We assumed a water density of 1.03 Mg/m^3, a sediment density of 2.2 Mg/m^3, a crust density of 2.7 Mg/m^3, and a mantle density of 3.3 Mg/m^3.

The resulting mantle Bouguer anomaly is then interpreted in terms of deviations from this reference model.

In our gravity study we used a one-layer, crustal model of constant thickness and density. In fact, *Morris and Detrick* [1991] have shown that there is only a 1-mGal difference with a two-layer crustal model (1500 m and 4500 m in thickness and 2.7 Mg/m^3 and 2.9 Mg/m^3 in density, respectively). Because this is of the same order of magnitude as the accuracy of our data, we have neglected this contribution. However, we do take into account the presence of sediment in the oldest basins, because, for example, a sediment thickness of 400 m creates a gravitational effect of 5 mGal (Figure 4b).

Mantle Bouguer Anomaly

The mantle Bouguer anomaly (MBA) (Figure 4c) was obtained by subtracting from the free-air anomaly the gravity effect computed from the above crustal model. The resulting amplitudes of the anomalies range from -40 to

Plate 1. (opposite) (a) Bathymetric color map contoured (contour interval is 200m). The map was constructed by interpolating the data onto a grid with a spacing of 2.8 km to minimize interpolation artifacts [*Inoue*, 1986]. We have superimposed the isochrons determined after anomaly magnetic identification and plate reconstruction as dotted lines [*Sloan and Patriat*, 1992]. The arrows on each side of the map indicate the location of line 29 shown in Figure 2. (b) Free-air gravity anomaly color map (contour interval is 5 mGal). The map was constructed like the bathymetric map. Note the good correlation between the anomaly patterns and the bathymetric features in Plate 1a.

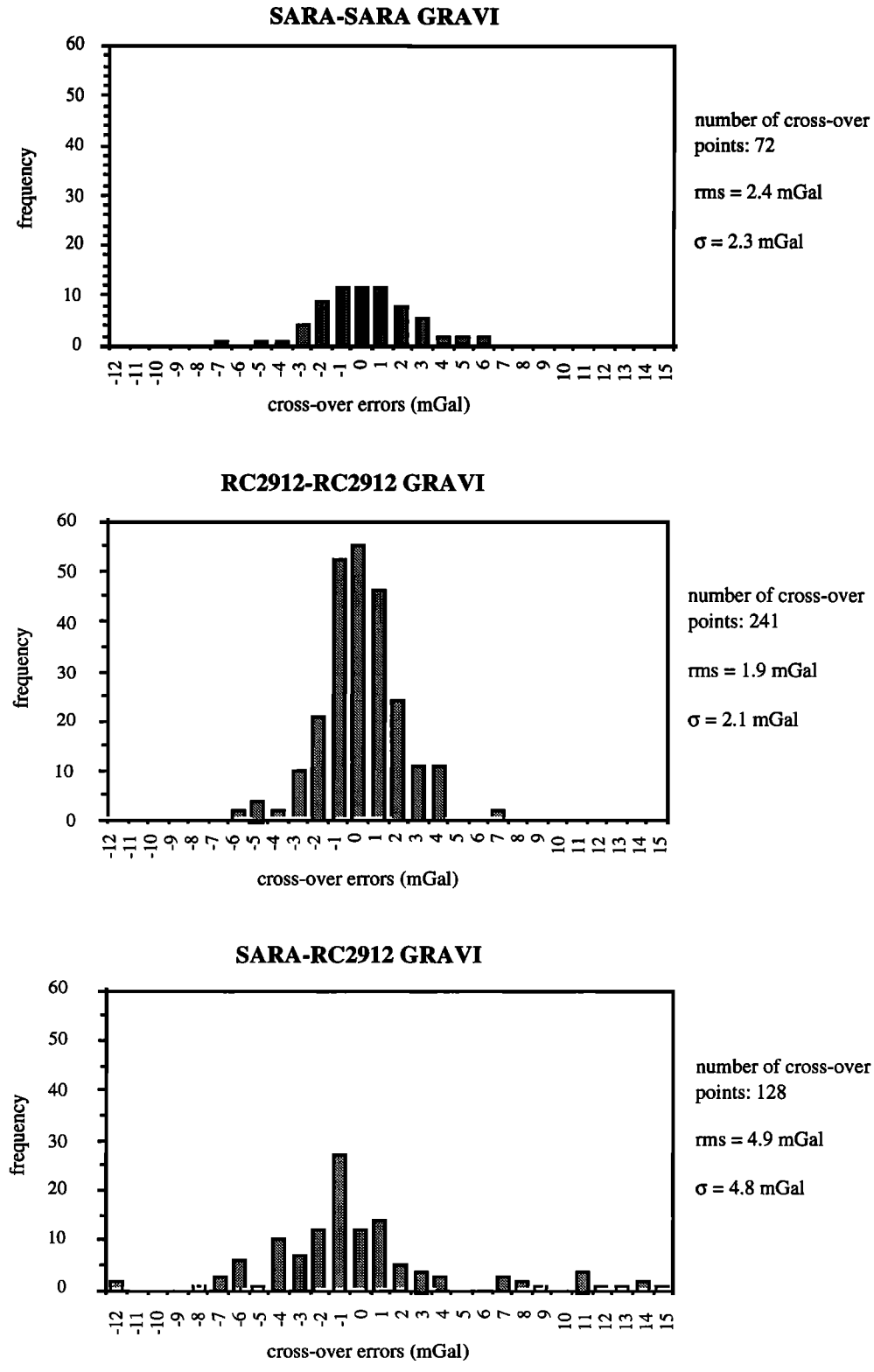

Fig. 3. Histogram of cross-over errors of free-air anomaly for both SARA and RC2912 cruises. There are 72 cross-over points for the SARA cruise, 241 cross-over points for the RC2912 cruise, and 128 cross-over points between SARA and RC2912 cruises. The respective rms, misfit, and standard deviation are written on each diagram.

+40 mGal (the zero level is arbitrary as previously explained). The MBA is no longer directly correlated with the topography. Along the axis, "bulls eye" gravity lows (labels A and B in Figure 4c) are centered on the spreading segments, as previously observed by *Lin et al.* [1990]. Off-axis, relative minima and maxima of the MBA are correlated with the ridge axis segment centers and the NTDs, respectively. However, the regional trend of the gravity anomaly is dominated by the effects of the cooling and deepening of the lithosphere with age which cause the MBA to increase away from the axis. Therefore it is necessary to account for this lithospheric effect before interpreting the anomalies.

Thermal Model

Variations in density occur in the upper mantle due to lithospheric cooling and thickening with age. Two different models are used and compared to determine this thermal effect.

In the first method, we used the mantle temperature structure calculated from a model of three-dimensional viscous flow driven by the separation of the overriding lithospheric plates [*Phipps Morgan and Forsyth*, 1988]. This flow model requires that the ridge axis geometry be described by orthogonal segments and transforms and assumes a fixed axial geometry (i.e., symmetric spreading) and constant spreading rate (12.5 mm/yr). The temperature field induced by the three-dimensional flow in the upper 100 km of the mantle is solved using a finite difference method. The temperature at the bottom and top of the grid are ascribed to 0°C and 1310°C, respectively. The temperature field in each discrete horizontal layer defined by the finite difference grid is converted into density variations using a coefficient of thermal expansion of $3.\ 10^{-5}$ $°K^{-1}$, and then converted into the gravity signal observed at the sea surface [*Kuo and Forsyth*, 1988].

In the second model, we computed the gravity effect resulting from the depth variations of the lithosphere/asthenosphere boundary. The deepening of this interface with age can be described as due to the cooling of a half-space, assuming that horizontal heat conduction is negligible compared with vertical heat conduction [*Parsons and Sclater*, 1977; *Turcotte and Schubert*, 1982]. The depth of the lithosphere/asthenosphere boundary is given by

$$Y_L(t) = 2.32\sqrt{\kappa t}$$

where t is the age of the lithosphere in Ma and κ is the thermal diffusivity [*Parsons and Sclater*, 1977]. κ is assumed to be 1 mm^2/s, and the contrast of density at this interface is assumed to be -0.06 Mg/m^3. Magnetic anomaly identification [*Sloan and Patriat*, 1992] allows us to generate an age grid, and the two-dimensional parametrization allows us to determine on each grid point the lithospheric depth.

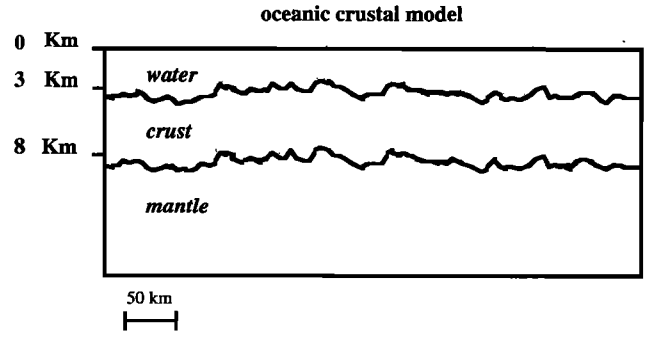

Fig. 4a. Model of the oceanic crust used in the mantle Bouguer anomaly computation. Sediments have not been represented because of the scale of the diagram. Densities of 1.03, 2.2, 2.7,and 3.3 Mg/m^3 were assumed respectively for seawater, sediments, crust, and mantle.

To compare the gravity effect resulting from the two methods and to test the validity of the second method, we first used, in this second model, the same assumption than in the first model (constant spreading rate of 12.5 mm/yr and fixed axis geometry). The difference between the gravity effect from the two models is less than ±2 mGal (of the same order as our data accuracy). Therefore, in case of small offsets at the NTDs as in the SARA area, the more complicated three-dimensional computation of method 1 is not necessary.

To investigate the influence of the evolution of the axial geometry with age, we have also computed the gravity effects of the cooling of the lithosphere using method 2 but taking into account the variations in spreading rate and direction deduced from magnetic anomaly identification and plate reconstruction [*Sloan and Patriat*, 1992]. Figure 5a shows the difference between the two thermal effects (model 1 minus model 2): differences are generally between ±2 mGal with extrema of about -4 and 4 mGal. The largest differences are observed along flow lines (about 8 mGal) and can be attributed to variations in the real spreading rate as opposed to the constant value assumed in method 1. Figure 5b displays the mean spreading rate used in model 1 and the "instantaneous" spreading rate used in model 2. From the present to anomaly 2 time and from anomaly 4 to anomaly 5 time, when the gravity difference between the two thermal models is positive, the instantaneous rate is faster than the mean rate, whereas it is smaller from anomaly 4 to anomaly 2 time, when the gravity difference is negative. Along isochrons, the variations are smaller (about ±2 mGal). Thus the main difference between these two thermal effects is observed along flow lines and appears to result from spreading rate variations. Therefore, although not a truly three-dimensional model, the lithosphere/asthenosphere boundary method constitutes our preferred method because it allows us to take into account the real pattern of lithospheric age.

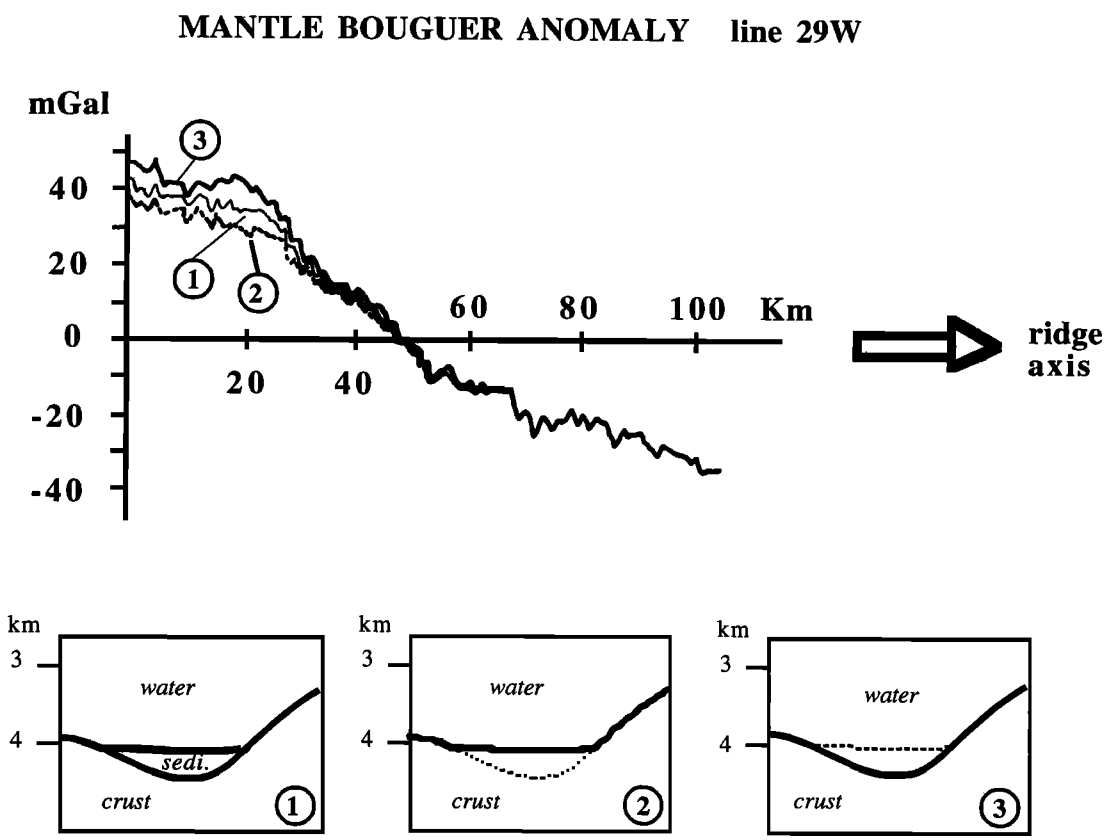

Fig. 4b. Computed gravity anomaly profiles along line 29W (see Plate 1a for location). The three curves correspond to three different crustal models. Solid line is crustal model 1 with three layers (sediment, crust, and mantle); dotted line is crustal model 2 where the top boundary is the seafloor; heavy solid line is crustal model 3 where the top boundary is the basement.

Residual Mantle Bouguer Anomaly

The gravity effect due to the deepening of the lithosphere/asthenosphere boundary was removed from the mantle Bouguer anomaly to obtain the residual gravity anomaly (RMBA; Plate 2a). The total amplitude of the anomalies ranges from -20 to +20 mGal (the zero level is arbitrary). The circular shape of the gravity anomaly lows at the axis is very similar to that obtained in a previous study of the ridge axis [*Lin et al.*, 1990]. On the flanks of the spreading axis we can follow three gravity maxima (yellow and green in Plate 2a) and three gravity minima (purple and blue in Plate 2a) which clearly highlight the configuration of the segmentation in the last 10 m.y. The relative maxima of anomalies are correlated with the bathymetric lows, i.e., the NTDs, and the relative minima of anomalies with the bathymetric highs, i.e. the centers of the segments. Between 28°40'N, 44°30'W and 28°10'N, 43°05'W, we can follow a RMBA low which corresponds to the appearance and growth of a new segment also observed in the bathymetric data in the form of a series of topographic highs parallel to the axis. These gravity results confirm that prior to anomaly 4a time, the structure of the ridge in our survey area consisted of two segments separated by one discontinuity with a gravity anomaly high and that subsequent to anomaly 4a the ridge consisted of three segments and two NTDs.

We have compared the segmentation of the MAR in our survey area, as defined by the bathymetry and the magnetic anomaly identification [*Sloan and Patriat*, 1992], with the segmentation defined by the gravity anomalies (Plate 2b). To a first order, the segmentation obtained from gravity anomalies is well correlated with the bathymetric and magnetic segmentation. This segmentation is characterized by a lozenge-shaped pattern, in plan view, of discordant zones on the flanks which do not follow plate motion flow lines, demonstrating that each segment advances and retreats continuously.

Crustal Thickness Modeling

The RMBA represents the part of the gravity field that cannot be explained by the predictable effect of seafloor topography, constant crustal thickness, or mantle density changes related to the cooling of the lithosphere. At the axis, the RMBA was interpreted as created by lateral variations in crustal or upper mantle density, differences in crustal thickness or some combination of these effects [*Lin et al.*, 1990; *Morris and Detrick*, 1991].

Profiles along isochrons, extracted from the three-dimensional, residual gravity anomaly map, reveal that the peak-to-trough amplitudes along the present axis and along the anomaly 4 isochron on both flanks are similar (about 20 mGal), and have the same wavelength,

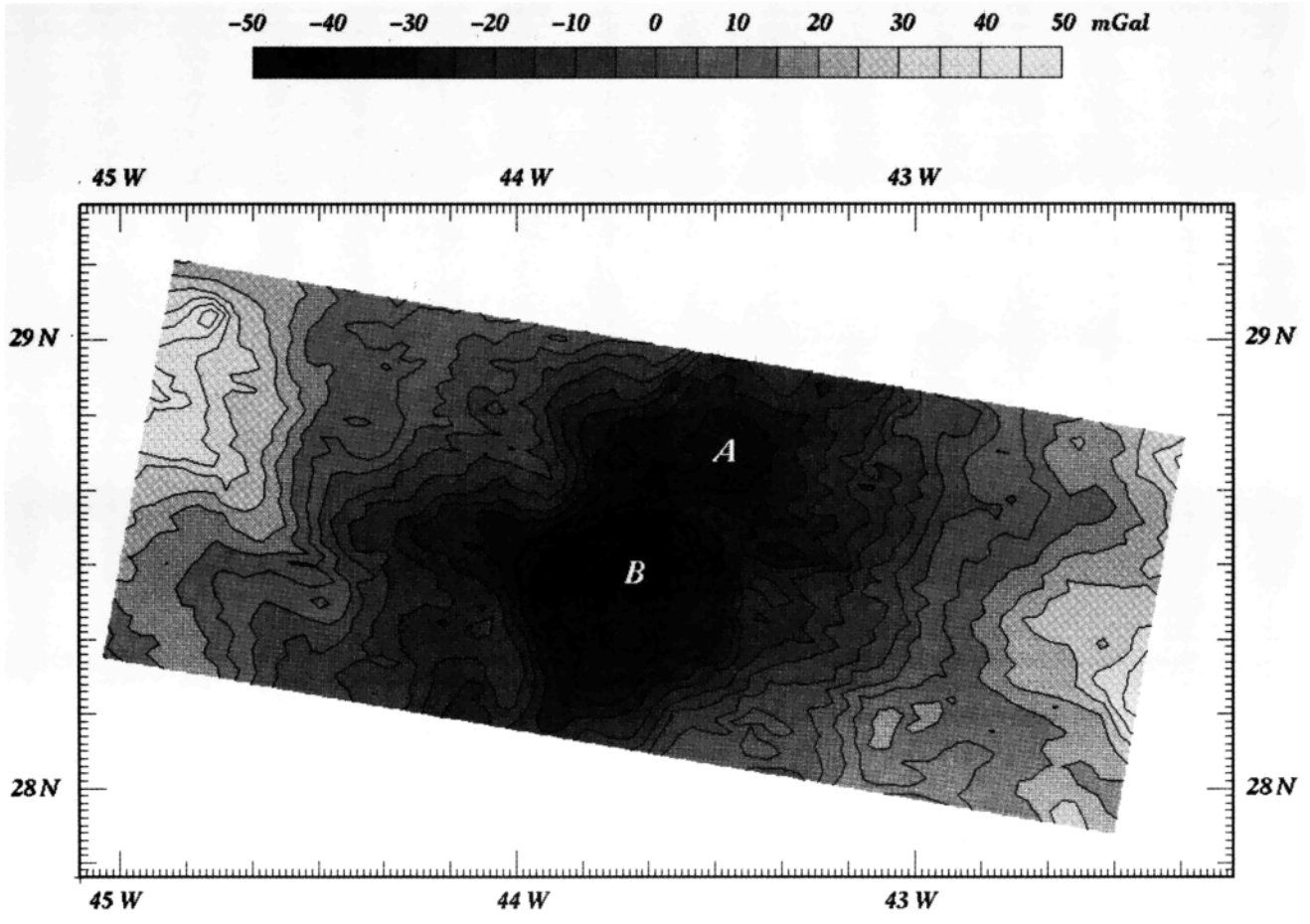

Fig.4c. Mantle Bouguer anomaly map (contour interval is 5 mGal). The zero level is arbitrary and corresponds to the mean value of the grid. Labels A and B represent "bulls eyes" gravity lows discussed in text. Solid line is relative MBA minima; dashed line is relative MBA maxima.

suggesting a similar origin for these gravity anomalies (Figure 6). A recent seismic refraction study along the Mid-Atlantic Ridge in the South Atlantic measured crustal thickness beneath two segment with particularly large "bull's eye" mantle Bouguer anomaly. The variations in crustal thickness obtained using these seismic data are of the correct magnitude to account for the observed gravity anomaly [*Tolstoy et al.*, 1992]. For these reasons, we interpret the residual anomalies in terms of along-axis, crustal thickness variations. To estimate these variations, we have downward continued the residual gravity anomalies to a constant depth of 8 km below sea level (average 3 km sea water and 5 km crust) following the method of *Kuo and Forsyth* [1988]. A cosine taper filter was applied to the residual anomalies to circumvent instability problems inherent in the downward continuation calculation at short wavelengths. This filter removes wavelengths less than 25 km, making sure that the sources of gravity anomaly are below the constant depth of 8 km. It cosine tapers the signal with wavelengths between 25 and 35 km and passes all wavelengths greater than 35 km. This low-pass filter smoothes out crustal thickness variations. The rms value of the misfit between the residual anomaly and the recomputed field is 2.31 mGal, which is comparable to the rms value of the cross-over errors of the free-air anomaly.

We observe that the variations in crustal thickness in the SARA area range from -1.5 to 1.5 km (Figure 7a). A general thinning of the oceanic crust from the axis to the flanks can be seen, suggesting that a long-wavelength component is still present in the RMBA. Although, a thicker crust on axis than on the flanks could indicate that melt production is more important at present than it was at anomaly 5, it is more likely that this effect is due to an inaccurate thermal model.

We have added the computed crustal thickness variations to our model of constant crustal thickness and calculated the gravity effect of this new crustal model to obtain a new residual gravity map (Figure 7b). The amplitudes of this recomputed anomalies range from -2 to +2 mGal. These short-wavelength (between 5 and 10 km) circular anomalies probably correspond to noisy data, but it is also possible that may correspond to outcrops of higher density rocks.

To summarize, the new crustal model fits observed data within noise level. Therefore, the crustal thickness variation is a possible interpretation of the RMBA.

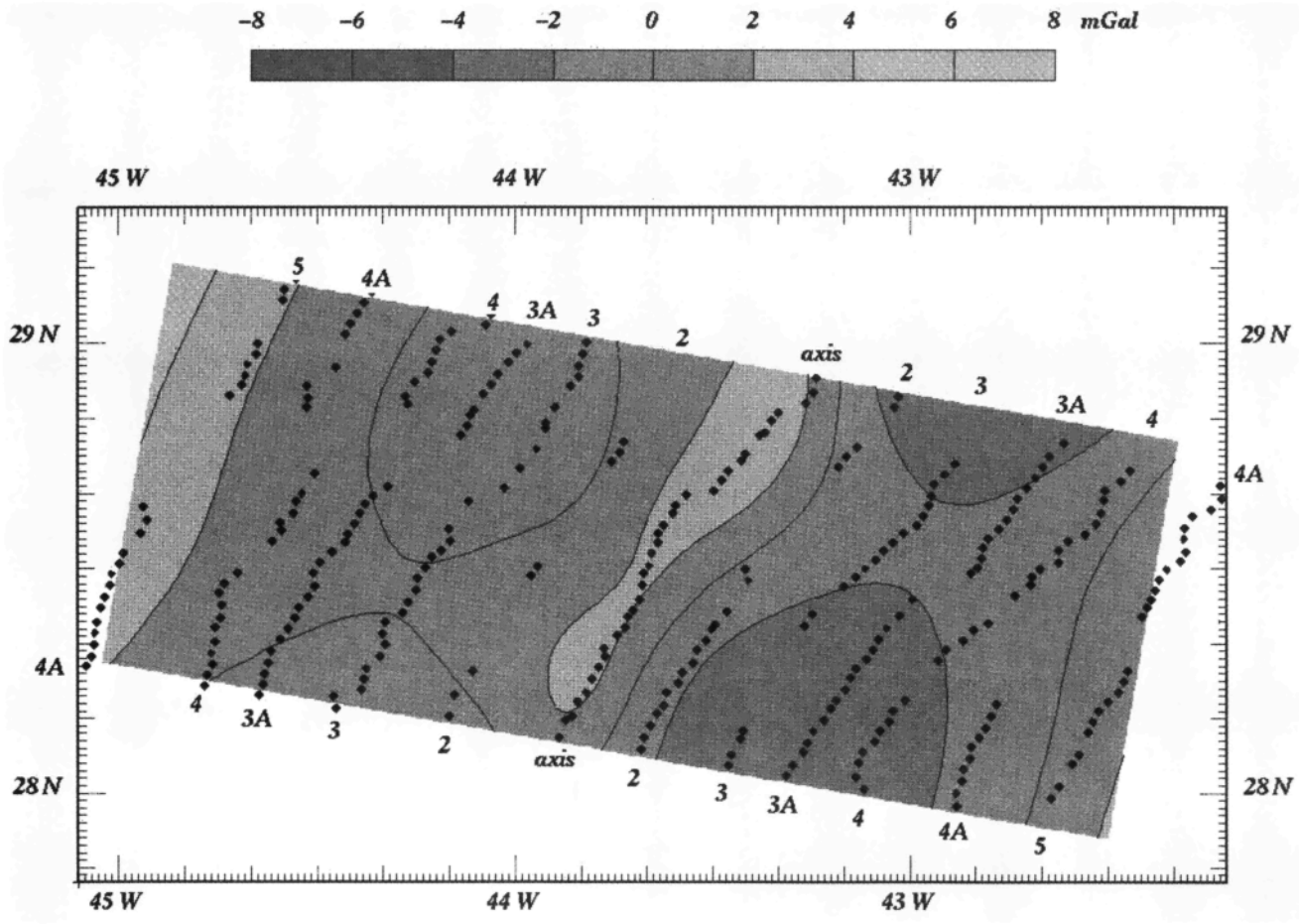

Fig. 5a. Map of difference between gravity effect due to model 1 (three-dimensional method of *Kuo and Forsyth* [1988]) and model 2 (half-space cooling model of *Parsons and Sclater* [1977]). Contour interval is 2 mGal. Isochrons have been superimposed as dotted lines.

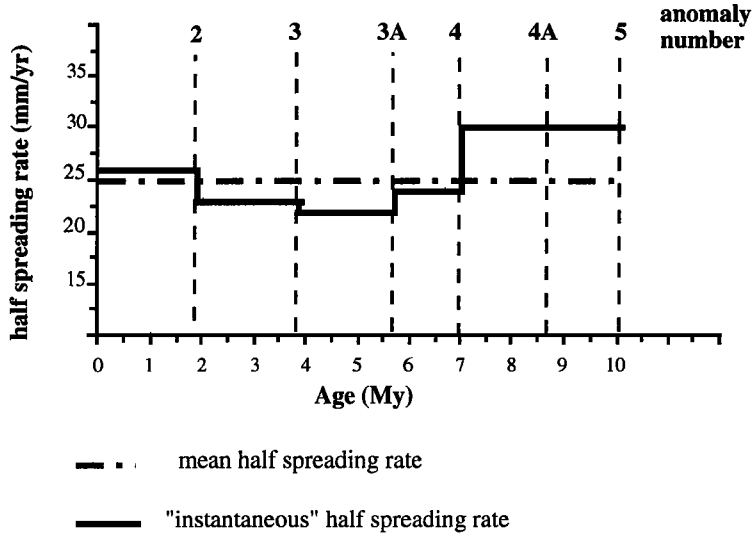

Fig. 5b. Comparison between spreading rates used in the two thermal models. Dashed line is mean spreading rate used in the first model; solid line is "instantaneous" spreading rate used in the second model.

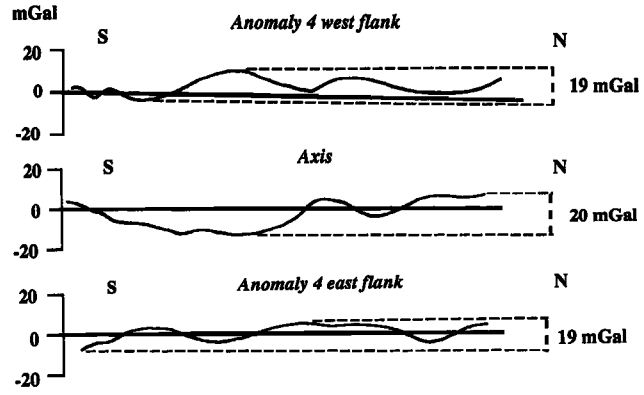

Fig. 6. Mantle Bouguer anomaly profiles along isochrons on the ridge axis and on the flanks at anomaly 4. Note the constant amplitude of anomalies between the axis and the flanks.

DISCUSSION

Comparison Between "Gravity" and "Bathymetric" Segmentation

We observe systematic northward and southward shifts (about 10 km) of the gravity traces of the nontransform discontinuities with respect to their bathymetric traces on the west and east flanks, respectively. The maximum of the gravity anomaly does not occur over the topographic basins which constitute the off-axis traces of the NTDs but over one of the walls bounding these traces. Such a shift has been observed over transform faults, where the maximum of the Bouguer anomaly is observed primarily over the walls of the fracture zone rather than over the center of the fracture zone valley [*Prince and Forsyth*, 1988]. A detailed study of bathymetry reveals that these basins are asymmetric: on the east flank, these basins are bounded by a gentle slope to the north and a steep escarpment to the south, while the converse is true on the west flank of the spreading center (Plate 2b). Assuming that the RMBA can be explained by variations in crustal thickness, this shift shows that the maximum and minimum depths of the Moho do not correspond to the topographic highs and basins respectively (Figure 8). It appears that the seafloor topography reflects the effect of intense tectonic deformation which does not affect all the crust. Therefore the trace of the segmentation may be partially offset by tectonic effect, while the Moho keeps the memory of the original segmentation.

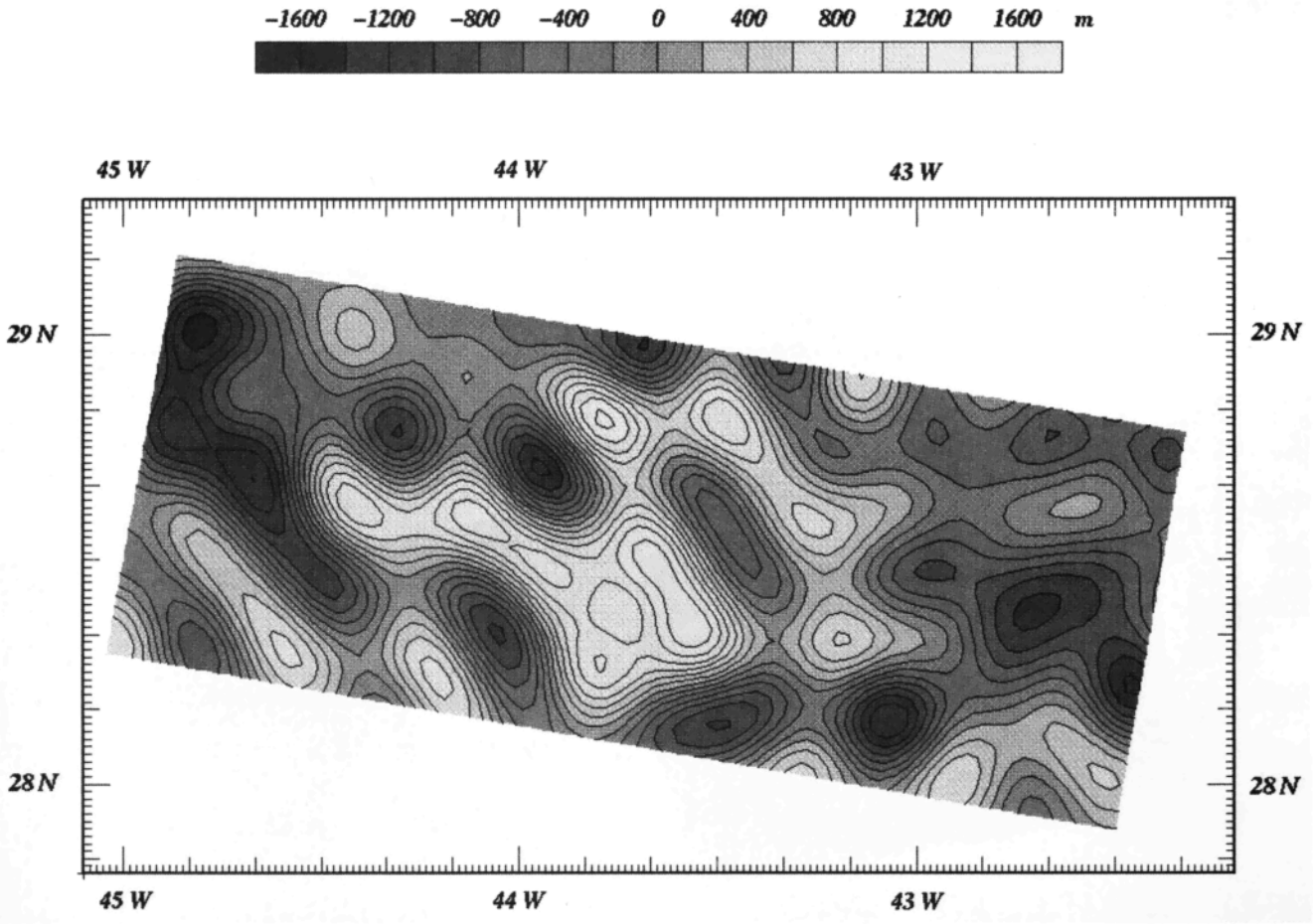

Fig. 7a. Map of variations in crustal thickness determined by downward continuation of the residual gravity anomalies to 8 km level. The contour interval is 200 m, and the values represent deviations from an assumed 5 km thick crust.

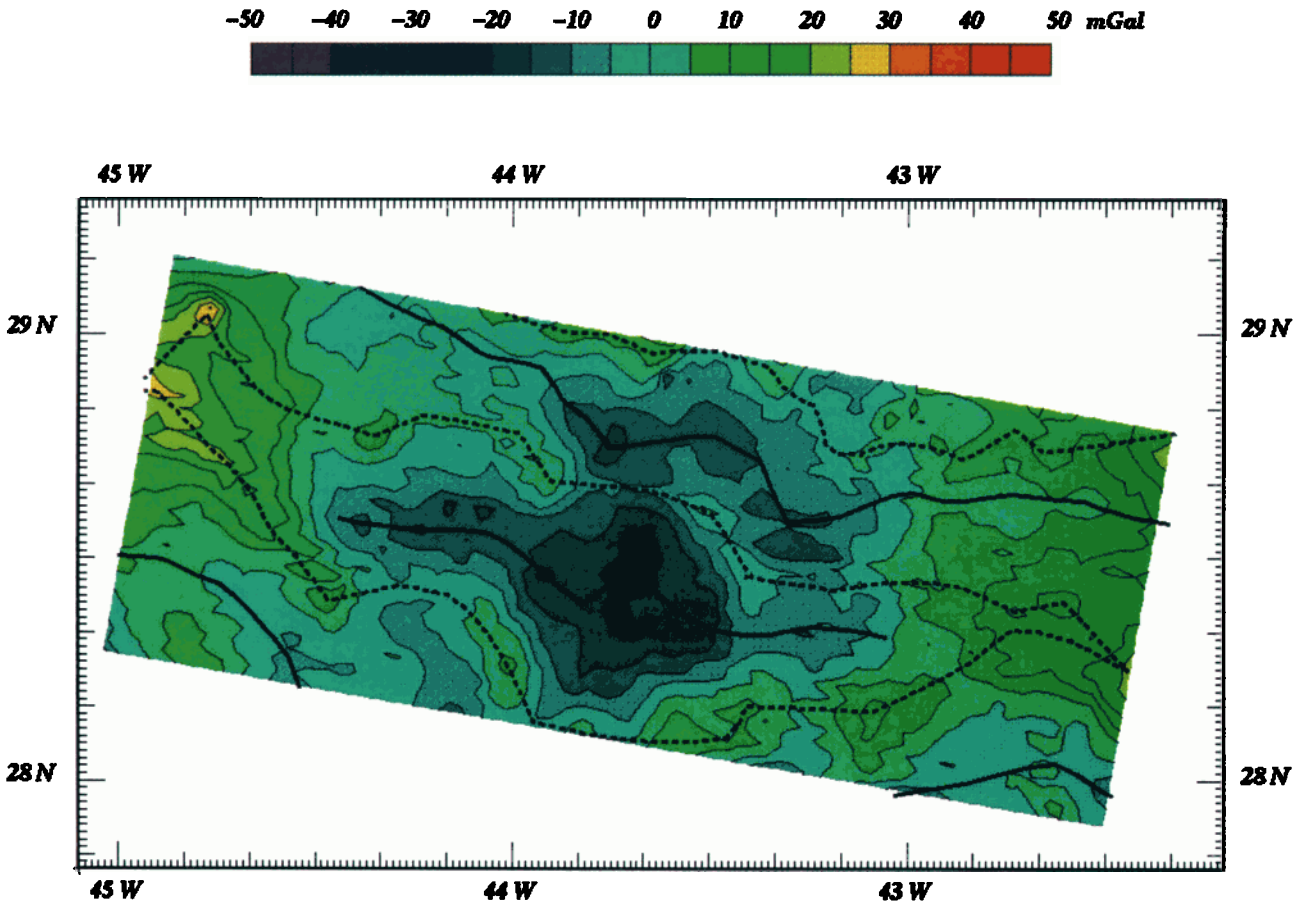
-50 -40 -30 -20 -10 0 10 20 30 40 50 mGal
45 W
44 W
43 W
29 N
28 N

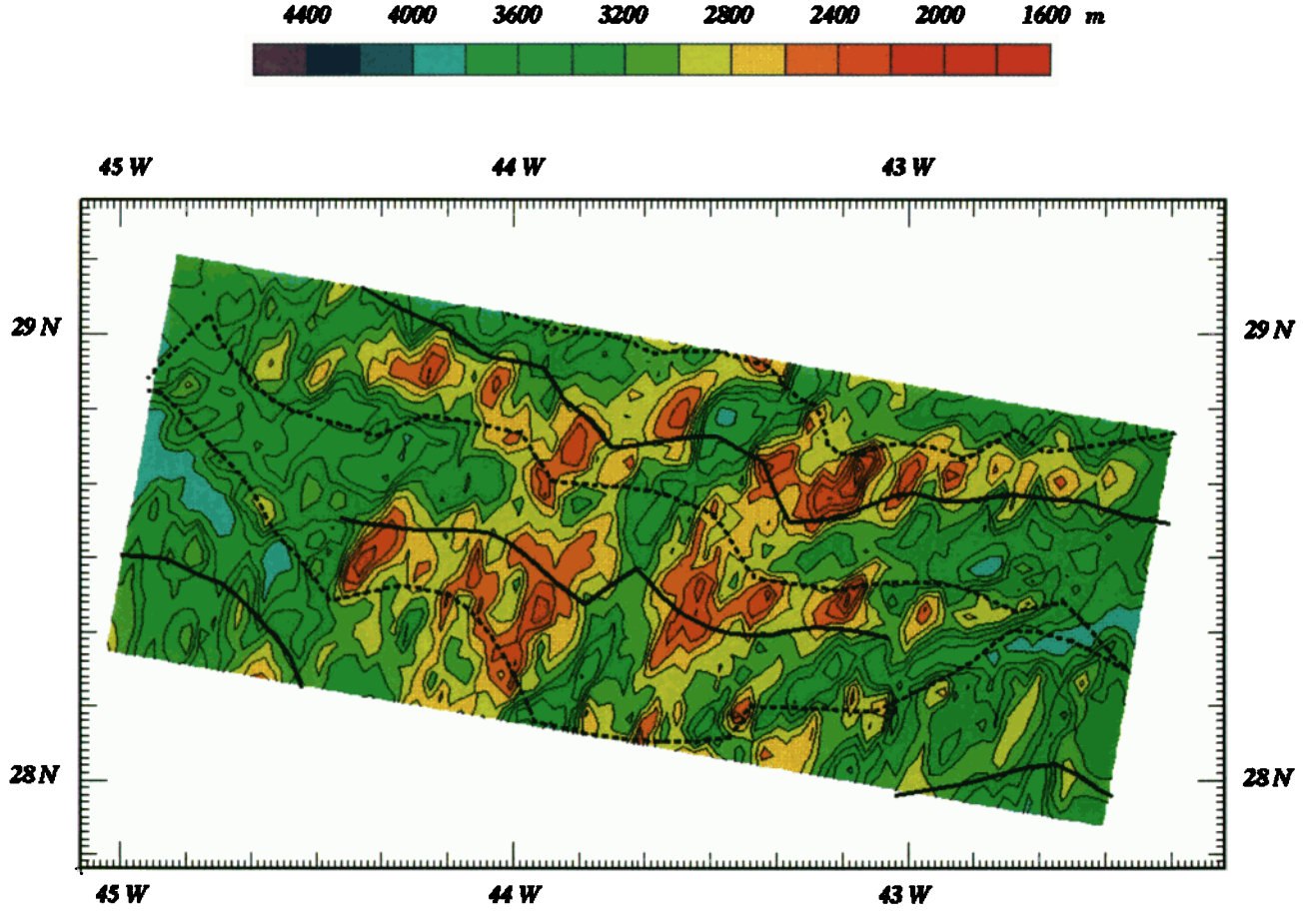
4400 4000 3600 3200 2800 2400 2000 1600 m
45 W
44 W
43 W
29 N
28 N

Short-Wavelength Residual Anomalies

The residual anomaly shown on Figure 7b is dominated by short-wavelength (5-10 km), positive anomalies, which we have interpreted in terms of noise. However, several of the features, already observed on the RMBA map, are located at the southward limit of topographic highs on the west flank (label A in Figure 7b) and at their northward limit on the east flank (label B in Figure 7b), i.e., the steep flanks of the basins. They correspond to local maxima of the free-air gravity anomaly which are not correlated with topographic highs. Because of their short wavelengths, they cannot have a deep-seated origin, and they cannot be interpreted in terms of crustal thickness variation. They may however correspond to massifs of rocks of higher densities than the mean crustal density, such as peridotite blocks. The size of the anomalies is consistent with peridotites outcrops previously observed along the Mid-Atlantic Ridge [*Mével et al.*, 1993; *Mével et al.*, 1991].

Ridge Flank Segmentation

The past segmentation of the Mid-Atlantic Ridge is defined by gravity traces of NTDs on the flanks of the

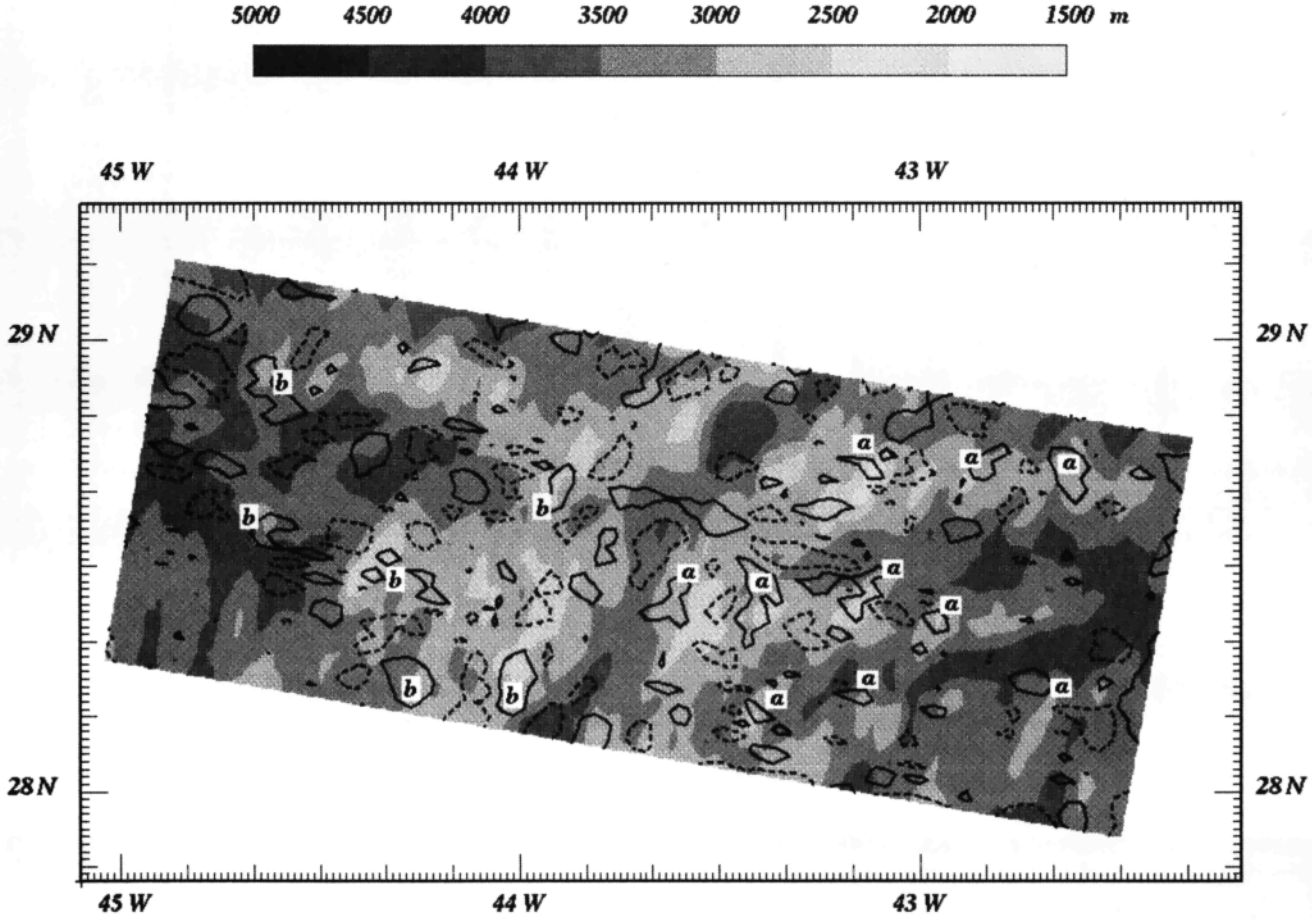

Fig. 7b. Residual gravity anomalies using a crustal model taking into account crustal thickness variations superimposed on the bathymetric map. Dotted lines: negative residual anomalies; solid lines: positive residual anomalies. Contour interval is 2 mGal. Note the location of positive anomalies (labels a and b) over the steep flanks of topographic highs.

Plate 2. (opposite) (a) Residual anomaly color map (contour interval is 5 mGal). This map was constructed by subtracting from the mantle Bouguer anomaly the attraction of the lithosphere/ asthenosphere boundary determined from the isochron map, and assuming densities of 3.3 and 3.24 Mg/m^3 for upper mantle and asthenosphere, respectively (model 2). Solid lines are the relative minima of gravity anomalies interpreted as the center of segment; dashed lines are the relative maxima of gravity anomalies interpreted as discontinuities. (b) Segment discontinuities (dashed lines) and center of segments (solid lines), as defined by the gravity study, superimposed on the bathymetric color map. We observe a systematic shift between the bathymetric discontinuities defined by V-shaped basins and the gravity discontinuities defined by the maximum of the anomaly.

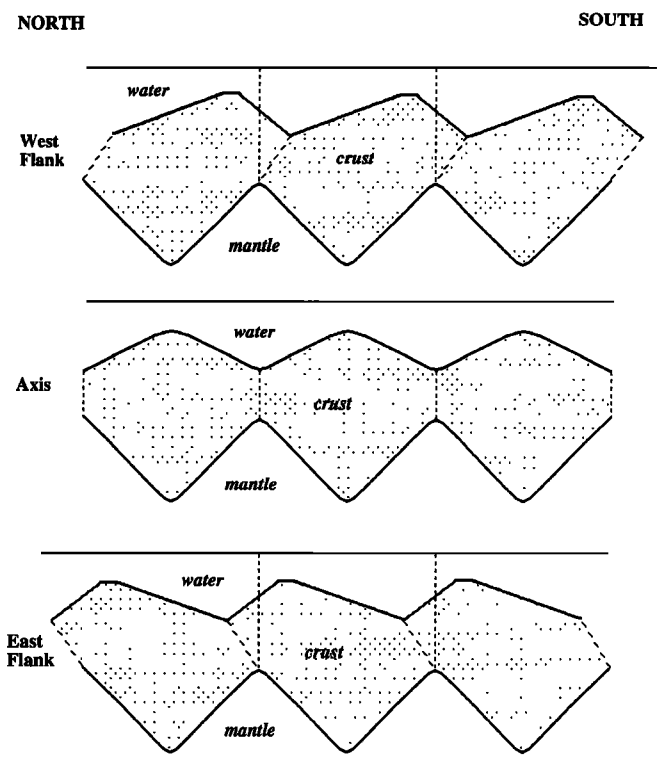

Fig. 8. Along-axis model of oceanic crust at the ridge axis and on the east and west flanks. The seafloor is obtained from the observed bathymetry and the Moho is defined from the gravity study. Minimum Moho depth does not occur beneath the basin but beneath the steep bounding side of the segment indicated by dashed lines.

spreading center (Plate 2b). On each flank, alternating areas of thick and thin crust, roughly parallel to the ridge axis, define a mosaic of crustal blocks, the limits of which are rings of thinner crust, with the former along-axis segmentation. This pattern may result from the temporal and spatial periodicity of mantle upwelling. The spatial periodicity, parallel to the axis, corresponds to the distribution of the center of segment, while the temporal variation, perpendicular to the axis, suggest that the magmatic supply may be more robust periodically, creating a thicker crustal block.

CONCLUSIONS

1. A striking feature of our gravity study is the persistence of mantle Bouguer anomalies on the ridge flanks. These anomalies allow us to study the evolution of the segmentation. They are characterized by anomaly lows over the center of the segments and anomaly highs over the discontinuities. This gravity segmentation shows that the length of the segments has varied with time, in agreement with bathymetric and magnetic studies.

2. A thermal model must take into account the successive geometry of the ridge axis and spreading rate variations.

3. There are systematic shifts off axis between residual mantle Bouguer anomaly highs and bathymetric lows. We propose that the fossil trace of the nontransform discontinuities is given by these gravity highs rather than by the bathymetric lows, which are the result of subsequent tectonic events.

4. The residual mantle Bouguer anomaly interpretation in terms of crustal thickness variations defines a mosaic of thicker crustal blocks limited by thinner crust, which could be the temporal and spatial trace of mantle upwelling or magma supply.

5. At short wavelengths, the interpretation in terms of crustal thickness variation allow us to define areas of densities higher than the mean crust density, which could indicate outcrop of high-density rocks such as peridotite.

Acknowledgments. We would like to thank A. P. Slootweg for providing us with useful computer programs for data representation and cross-over error computations and also for fruitful discussions about this paper. B. Cornaglia provided valuable assistance in the computational problems. In addition, discussions with L. Parson and L. Géli were greatly appreciated. Particular thanks to J. Pariso and S. Tait for their English corrections. We thank the officers, crew and scientific personnel of the R/V *Jean Charcot* (leg SARA) for their support at sea. We thank anonymous reviewers for helpful and critical reviews. This work was partially funded by IFREMER and CNRS-Institut National des Sciences de l'Univers DBT grant 91-559 *Thème Dynamique Globale*. This is DBT contribution 649.

REFERENCES

Chapman, M. E., Techniques for interpretation of geoïde anomalies, *J. Geophys. Res.*, *84*, 3793-3801, 1979.

Dubois, J., and C. Deplus, Gravimetry on the Erimo seamount, Japan, *Tectonophysics*, *160*, 267-275, 1989.

Inoue, H., A least-squares smooth fitting for irregularly spaced data: Finite-element approach using the cubic B-spline basis, *Geophysics*, *51*, 2051-2061, 1986.

Kuo, B. Y., and D. W. Forsyth, Gravity anomalies of the ridge-transform system in the South Atlantic between 31° and 34.5°S: Upwelling centers and variation in crustal thickness, *Mar. Geophy. Res.*, *10*, 205-232, 1988.

Lin, J., G. M. Purdy, H. Schouten, J. C. Sempéré, and C. Zervas, Evidence for focused magmatic accretion along the Mid-Atlantic Ridge, *Nature*, *344*, 627-632, 1990.

Macdonald, K. C., D. C. Scheirer, and S. M. Carbotte, Mid-ocean ridges: Discontinuities, segments and giant cracks, *Science*, *253*, 986-994, 1991.

Mével, C., M. Cannat, J. F. Casey, and J. A. Karson, Generation of oceanic lithosphere at slow spreading centers: Drilling in the western wall of the MARK area, *Proc. Ocean Drill. Program Initial Rep.*, in press, 1993.

Mével, C., M. Cannat, P. Gente, E. Marion, J. M. Auzende, and J. A. Karson, Emplacement of deep crustal and mantle rocks on the west median valley of the MARK area (MAR, 23°N), *Tectonophysics*, *190*, 31-53, 1991.

Morris, E., and R. S. Detrick, Three-dimentional analysis of

gravity anomalies in the MARK area, Mid-Atlantic ridge 23°N, *J. Geophys. Res.*, *96*, 4355-4366, 1991.

Parsons, B,. and J. G. Sclater, An analysis of the variation of ocean floor bathymetry and heat flow with age, *J. Geophys. Res.*, *82*, 803-827, 1977.

Patriat, P., C. Deplus, C. Rommevaux, H. Sloan, P. Hunter, and H. Brown, Evolution of the segmentation of the Mid-Atlantic Ridge between 28° and 29°N during the last 10 Ma: Preliminary results from SARA Cruise (R/V *Jean Charcot*, May 1990), *Eos Trans. AGU, 71, Fall Meeting suppl.*, 1629, 1990.

Phipps Morgan, J. P., and D. W. Forsyth, Three-dimensional flow and temperature perturbations due to a transform offset: effects on oceanic crustal and upper mantle structure, *J. Geophys. Res.*, *93*, 2955-2966, 1988.

Prince, R. A., and D. W. Forsyth, Horizontal extent of anomalously thin crust near the Vema fracture zone from the three-dimentional analysis of gravity anomalies, *J. Geophys. Res.*, *93*, 8051-8063, 1988.

Sempéré, J. C., G. M. Purdy, and H. Schouten, Segmentation of the Mid-Atlantic Ridge between 24°N and 30°40'N, *Nature*, *344*, 427-431, 1990.

Sloan, H., and P. Patriat, Kinematics of the North American-African plate boundary between 28° and 29° N during the last 10 My: Evolution of the axial geometry and spreading rate and direction, *Earth Planet. Sci. Lett.*, *113*, 323-341, 1992.

Tolstoy, M., A. J. Harding, and J. A. Orcutt, An explanation for "bull's Eye" mantle Bouguer anomalies on the southern Mid-Atlantic Ridge, *Eos Trans. AGU, 73 (43), Fall Meeting suppl.*, 495, 1992.

Turcotte, D. L., and G. Schubert, Heat transfer, in *Geodynamics: Applications of Continuum Physics to Geological Problems*, pp. 135-197, John Wiley, New York, 1982.

C. Deplus, P. Patriat, and C. Rommevaux, Institut de Physique du Globe, 4 place Jussieu, boîte 89, 75252 Paris Cedex 05, France.

J.-C. Sempéré, School of Oceanography, WB-10, University of Washington, Seattle, WA 98195.

(Received December 7, 1992;
revised July 22, 1993;
accepted August 20, 1993.)